One-dimensional freezing of nonheaving unsaturated soils: Model formulation and similarity solution

Aleksey Y. Sheshukov[1] and John L. Nieber[2]

Received 6 February 2011; revised 26 September 2011; accepted 8 October 2011; published 18 November 2011.

[1] Freezing of unsaturated soils is associated with the formation of a moving freezing zone and liquid water flow toward the zone. An equilibrium thermodynamic formulation of coupled flow and heat transport in variably saturated partially frozen porous media is developed and a self-similar solution is derived for the case of a semi-infinite horizontal porous media column with a constant freezing temperature on one boundary. Solutions to the self-similar equations are derived using a Runge-Kutta solution procedure. The solution is found to yield two possible modes distinguished by zones composed of different combinations of ice, liquid water, and air. One of the modes contains three zones: a frozen zone (WI) with just ice and liquid water; a transition zone (AWI) with ice, liquid water, and air; and an unsaturated zone (AW) with liquid water and air. The second mode contains only the WI zone and the AW zone. It is found that the WI zone is a quintessential part of the solution. The AWI zone is found to exist when the advancement of the freezing zone is relatively fast, while it is absent when the zone advances slowly. Predictions of ice saturation and liquid water saturation with the self-similar solution are compared to published experimental data. Pore pressure is calculated as a linear combination of ice pressure and liquid water pressure, and the calculated figures are used to provide a condition for model limitation in the case of incipient ice lens formation. The developed similarity solution provides insight into the mechanics of liquid water movement and pore filling with ice and the conditions for incipient heaving.

Citation: Sheshukov, A. Y., and J. L. Nieber (2011), One-dimensional freezing of nonheaving unsaturated soils: Model formulation and similarity solution, *Water Resour. Res., 47*, W11519, doi:10.1029/2011WR010512.

1. Introduction

[2] The majority of unsaturated soils in northern regions are subject to freeze-thaw cycles. Freezing of soils due to applied subzero temperature at the soil surface results in the formation of a freezing front that progresses downward with time. The reduced liquid water content and liquid water pressure at and behind the freezing front induce water flow toward the zone behind the front and accumulation of ice therein. While freezing persists and progresses downward, more water is drawn from deeper horizons, increasing pore pressure behind the freezing front [*Harlan*, 1973]. When the pore pressure behind the freezing front exceeds the overburden pressure, the matrix structure at that point in the soil will break, thus allowing initiation of a pure ice layer or an ice lens. This lens then continues to accumulate ice as liquid water transfers toward it, thereby uplifting the soil above that depth and causing frost heave [*O'Neill and Miller*, 1985]. While frost heave had been an important subject of interest for scientists and civil engineers for years because of the practical relevance, especially in permafrost regions, research on the overall process of freezing in soils even without a noticeable frost heave is of interest for hydrologists with regard to the water balance of soils and the redistribution of water and dissolved constituents in the soil during cold seasons [*Matzner and Borken*, 2008]. For example, melting snow and ice releases water, which infiltrates and percolates downward and supplies groundwater reservoirs, lakes, and rivers. Also, the permeability of frozen soils, being significantly lowered due to ice-occupied parts of the available pore void, reduces the infiltration rate and increases surface runoff [*Cherkauer and Lettenmaier*, 1999].

[3] The first studies on freezing of soil were published in the 1930s and include papers by *Taber* [1930] and *Beskow* [1935]. Starting in the 1970s, the research involved numerous experimental and theoretical studies with simultaneous heat transfer and water mass redistribution and associated phase change. Various models with different degrees of complexity have been developed [*Cary and Mayland*, 1972; *Harlan*, 1973; *Guymon and Luthin*, 1974; *Taylor and Luthin*, 1978; *Flerchinger and Saxton*, 1989]. The models contain temperature, water pressure, and water and ice saturations as the main variables. An equilibrium thermodynamics approach was used to provide the required closure relationships between the variables in the majority of these models [*Koopmans and Miller*, 1966; *Miller*, 1980; *Spaans and Baker*, 1996], while a nonequilibrium formulation was utilized by *Bronfenbrener and Korin* [1999]. *Harlan* [1973]

[1]Department of Biological and Agricultural Engineering, Kansas State University, Manhattan, Kansas, USA.
[2]Department of Bioproducts and Biosystems Engineering, University of Minnesota, Twin Cities, Saint Paul, Minnesota, USA.

0043-1397/11/2011WR010512

presented a system of mass and heat transport equations to model water and temperature redistribution during freezing of a soil column. The models based on *Harlan*'s [1973] approach supplement the transport equations with a closure condition that provides relationships between temperature, unfrozen water content, and water pressure. The closure condition can be derived using the equilibrium thermodynamic approach [*Kung and Steenhuis*, 1986; *Newman and Wilson*, 1997; *Zhao et al.*, 1997; *Shoop and Bigl*, 1997] or approximated on the basis of the experimental measurements of temperature and unfrozen water content [*Engelmark and Svensson*, 1993; *Daanen et al.*, 2007]. These models have facilitated numerical modeling studies of soil freezing [*Jame and Norum*, 1980; *Newman and Wilson*, 1997; *Hansson et al.*, 2004; *Daanen et al.*, 2007; *Li et al.*, 2009]. The contribution of the vapor phase on heat and mass balance was included by *Kung and Steenhuis* [1986] and *Flerchinger and Saxton* [1989]. The models cited above provided analyses of freezing behavior without frost heave in soils and therefore did not include conditions at which the transition to frozen saturated soils becomes possible. Without such a condition, there is nothing to prevent the ice content from exceeding soil porosity and invalidating the physical applicability of the model. In this paper we seek a formulation that is valid for freezing in both unsaturated and saturated, frozen and unfrozen soils.

[4] Among laboratory experiments, the studies by *Dirksen and Miller* [1966] and *Jame and Norum* [1980] were conducted on freezing of initially unsaturated horizontal soil columns. Boundary conditions were kept constant, and total moisture and temperature distributions were recorded at several time intervals. In each experiment the freezing front was observed to form soon after the beginning of the experiment, and water content was decreased with time in the warmer side of the column. These results are the only data available for validation and have been utilized in a number of numerical studies [*Kung and Steenhuis*, 1986; *Engelmark and Svensson*, 1993; *Newman and Wilson*, 1997; *Daanen et al.*, 2007].

[5] Since analytical solutions are hard to obtain because of the highly nonlinear nature of the governing equations, solutions of simplified formulations become of value. Similarity solutions present a substantial way of reducing the number of variables and solving the boundary-value problem for ordinary, not partial, differential equations. Moreover, in a self-similar coordinate $xt^{-1/2}$, the problem becomes time independent, which allows an easier way to investigate qualitative features of the model, as shown by *Lombardi and Tarzia* [2001] for thawing of saturated porous medium. The system of equations originally presented by *Harlan* [1973] is self-similar if the freezing is applied to a horizontal semi-infinite soil column with constant temperature and a no-flow boundary condition at the freezing end.

[6] Our focus in this paper is to present a concise description of the morphological structures for the ice, liquid water, and air content distributions and associated liquid water movement and coupled heat transport in a nonheaving porous media column during freezing. We limit the analysis to nonheaving conditions to keep the analysis simpler, to focus on the freezing processes alone without the complexities of frost heave deformation processes, and to seek a problem formulation that is amenable to the self-similar solution. Thus, the main objectives of this paper are to present a mathematical formulation that is capable of describing heat and mass transport for freezing of partially saturated, partially frozen nonheaving soils, to develop a similarity solution for freezing of horizontal initially unfrozen unsaturated soil, and to use the solution to provide quantitative analysis of the prevailing freezing processes, the resulting morphological structures, and the model limitations associated with incipient heaving.

[7] The paper is organized as follows. In section 2, we introduce the formulation and derive closure relationships with the assumption of thermodynamic equilibrium. The physical settings of the system that allow a similarity solution are presented and a dimensionless mathematical model is developed in section 3. In section 4, we provide a qualitative analysis of the model and construct possible modes of the solution. Numerical results and a discussion of various modes are presented in section 5, and a comparison with experimental observations is illustrated in section 6. The morphology of the freezing zone and the calculation of pore pressures are discussed in section 7, along with a discussion of the limitation of the ice pressure model. Section 8 summarizes our main conclusions.

2. Theory

[8] The conceptual idea of the progression of freezing in an unsaturated soil can be described by considering an initially uniformly moist column of unsaturated porous media in horizontal orientation. In addition to being initially uniformly moist, the column is initially at uniform temperature above the freezing point of pure water at the prevailing unsaturated state. The column is then subjected to a freezing temperature on the left end, while on the right end the temperature and moisture content are held steady at their initial values. The left boundary is impermeable to liquid water flow. Upon initiation of freezing, the freezing will progress to the right, while liquid water will move from the right toward the zone where freezing occurs. With the formation of ice in the pores, up to three distinct zones form in the column, as will be shown in the theoretical and mathematical analysis to follow. One zone, the one closest to the freezing boundary, will have pores completely filled with ice and liquid water; that is, the air will no longer be present. We refer to this as the WI zone. A second zone, one with liquid water and air and no ice, will exist to the right. We will refer to this one as the AW zone. One other possible zone can exist depending on the freezing rate and porous media properties, and that zone will have ice, liquid water, and air present. This zone, referred to as the AWI zone, if it exists, will occur between the WI zone and the AW zone. The configuration of air, water, and ice in the porous medium can be viewed at the pore scale using the theoretical concepts presented by *Miller* [1973].

[9] A diagram relating the equilibrium state of the ice–liquid water–air at the pore scale [*Miller*, 1973, 1980] is illustrated in Figure 1, which also shows the core-scale saturations of liquid water, ice, and air within the porous medium as related to temperature. The core-scale plot is the porous medium volume average representation of the same equilibrium states shown for the pore scale. Six principal states of the freezing process are distinguished by two

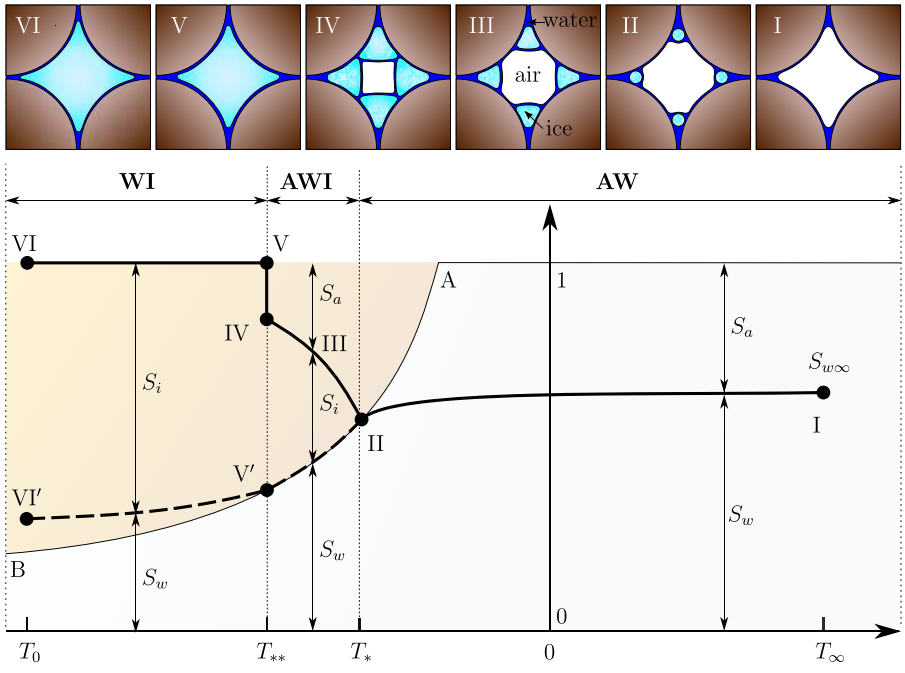

Figure 1. (top) A pore-scale diagram of six key equilibrium states during the freezing process and (bottom) the core-scale saturations of unfrozen water, ice, and air within the porous medium at the same equilibrium states in the corresponding pore-scale representation. The core-scale plot represents the volume-averaged quantities for a porous media. Changes in the saturations are shown by the solid and dashed lines, with the key states indicated by the solid circles and numbered from I to VI. Labels for the states are as follows: I, no ice; II, stable ice crystal forms; III, growth of ice crystal in crevice and pore throat; IV, threshold to filling pore with ice; V, pore filled with ice with liquid water as films and crevice edges; VI, continued ice formation into smallest spaces. Values of T_* and T_{**} represent two critical temperatures at which the inception of ice grain formation or collapse of the air space, respectively occur during the freezing process. The zone diagram in the $S_w(T)$ plane is divided into two domains by the line A-B, which is the line given by the equilibrium relation (11). The AWI zone occurs along this equilibrium curve, while zones AW and WI occur when values of S_w and T belong to the domain to the right or to the left of the AWI curve, respectively.

critical temperatures T_* and T_{**} and are presented in the saturation-temperature plane as well as in the corresponding pore-scale diagrams. The initial unfrozen porous medium is at a temperature above the freezing point and is shown by the solid point labeled I. At the pore scale, only air and the liquid water will be present in the pore space, as seen in pore-scale diagram I. As temperature decreases to a critical temperature T_*, a stable ice grain will form in the liquid-filled crevices of the pore, as shown in pore-scale diagram II. That critical point II and the decrease in liquid water content while moving from I to II are also shown on the graph for the core-scale. As temperature continues to decrease, the initially formed ice grain will continue to grow, as shown in pore-scale diagram III, further increasing the ice content and decreasing the liquid water content. This continued ice growth assumes that a liquid water supply is connected to the pore through the liquid-filled crevices. In a soil that water supply would be from water flowing to the pore from other pores containing liquid that are at a higher temperature. At a second critical temperature given by T_{**} the growing ice grain will suddenly grow to fill the entire pore space, forcing out the resident air by drawing in liquid water and freezing it, as seen in pore-scale diagrams IV and V. This last condition is seen as a sudden jump in the ice content of the core presented in the core-scale graph by the transition from state IV to state V. The sudden change in total water saturation between states IV and V is due to a drop in air content and a sudden increase in ice content and is not due to an increase in liquid water content. Each of these states of ice content is an equilibrium state based on the first law of thermodynamics and can be described by the generalized Clapeyron equation, which will be presented in section 2.3. The decrease in temperature from T_{**} causes further freezing of water in the system that does not contain air, as illustrated by pore diagram VI. Expansion of ice due to freezing forces water out of the pore space, and this means that water will flow in the direction of the warmer region. While total water saturation remains at the maximum value of unity during the transition from V to VI, the liquid water saturation decreases, as shown by the dashed line V′–VI′.

[10] We will define two key morphological characteristics of the freezing zone (between points II and IV, the AWI zone) for the sake of reference. Some freezing also occurs in the zone behind IV, but the amount of ice formation is small compared to the ice formation in the zone

between II and IV. The leading edge of the freezing zone will be referred to as the front of the freezing zone, and this corresponds to the leading edge of pore water freezing at point II. The trailing edge of the freezing zone exists at point IV and will be referred to as the tail of the freezing zone. For some initial and boundary conditions the AWI zone will not exist; that is, points II and IV coincide, but even then the ice formation occurs but at a point instead of over a finite distance.

[11] Each of the aforementioned zones, WI, AWI, and AW, are outlined in the core-scale diagram in Figure 1. Whether or not the AWI zone will exist in a porous medium will depend on the characteristics of the porous medium and on the rate of advancement of the leading freezing front. If the advancement rate is slow enough, the AWI zone can be completely suppressed, and state II coincides with state IV. For this case the front and the tail of the freezing zone coincide with each other.

[12] In the analysis to follow the freezing soil column is assumed to be rigid, isotropic, and homogeneous and in horizontal orientation. Following an approach developed by *Harlan* [1973] and adopted in other studies, the mathematical model developed is based on the principles of mass and thermal energy conservation, supplemented by equilibrium relations appropriate for each zone. The assumption of a rigid porous medium means that the medium will remain intact even with a large rise in ice pressure, and therefore, ice lens formation and frost heave are not considered in the analysis. The main focus of the analysis is to evaluate the processes of liquid water movement to the freezing zone and the accumulation of ice within and behind that zone, along with the increase of ice pressure within the WI zone. The effects of this ice pressure buildup on the liquid water flux are also of interest. The phenomenon of ice lens formation in freezing porous media is of interest to us, but the associated analysis will be relegated to future analyses.

2.1. Balance Equations

[13] During freezing, a pore void may be occupied by water (subscript w), air (a), and ice (i), simultaneously, and hereby the corresponding core-scale saturations S are subject to the constraint

$$S_w + S_i + S_a = 1. \tag{1}$$

[14] The balance equation for total mass of water present in both liquid and solid phases may be expressed as

$$\phi \frac{\partial}{\partial t}(\rho_w S_w + \rho_i S_i) + \rho_w \frac{\partial q}{\partial x} = 0, \tag{2}$$

where t is the time, x is the spatial coordinate positive downward, ϕ is the porosity, ρ_w and ρ_i are the density of liquid water and ice, respectively, and q is the water flux. We note that ice is considered immobile and a possible ice propagation could occur only through the regelation process of water freezing and ice melting.

[15] Adopting the similarities between ice-free and air-free conditions in soil leads to the flow of water in freezing soils being described by the same principles as the flow in unfrozen unsaturated soils, with the flow driven by gradients in water pressure heads ψ_w and the gravitational potential head. For this Darcy's law for flow is assumed to apply:

$$q = -K \frac{\partial \psi_w}{\partial x} + K, \tag{3}$$

with the hydraulic conductivity function K being dependent on both water and ice saturations as

$$K = K_s S_w^{2b+3} 10^{-E\phi S_i}. \tag{4}$$

Here K_s is the saturated hydraulic conductivity, and b is the pore size distribution index. The first term in (4) is the Brooks and Corey model [*Brooks and Corey*, 1966] developed for ice-free unsaturated soils media. *Jame and Norum* [1980] noticed and later *Nakano et al.* [1983] experimentally demonstrated that ice accumulation within pore voids can contribute to significant decreases in the ability of liquid water to flow through partially frozen porous media. To accommodate the effect of restriction of flow paths due to ice blockage of pores, the second term in the hydraulic conductivity function in (4) was introduced by *Taylor and Luthin* [1978]. The empirical constant E, called the impedance factor, should be calibrated with available data from experiments.

[16] The energy balance equation can be written for freezing soils as

$$\frac{\partial}{\partial t}(C_m T) - \phi \rho_i L \frac{\partial S_i}{\partial t} + C_w \frac{\partial}{\partial x}(qT) = \frac{\partial}{\partial x}\left(\lambda_m \frac{\partial T}{\partial x}\right), \tag{5}$$

where C_m and C_w are the bulk and liquid water volumetric heat capacity, respectively, λ is the thermal conductivity, and L is the latent heat of freezing. The second term on the left-hand side of (5) represents change in energy due to the latent heat released during freezing. The heat capacity and thermal conductivity of the medium denoted by the subscript m may be functions of pore content and soil properties.

[17] With proper constitutive relationships describing physical and hydraulic properties of the medium, the system of equations (1)–(5) is valid within the AW, AWI, or WI zones. In sections 2.2–2.4, supplemental equilibrium relationships for each of the three possible zones are discussed and presented.

2.2. Unsaturated Unfrozen Zone (AW Zone)

[18] The AW zone represents an ice-free unsaturated soil that leads to zero ice saturation and hence zero ice pressure ψ_i:

$$S_i = 0, \qquad \psi_i = 0. \tag{6}$$

Equation (6) eliminates input of ice in the energy and mass balance equations and transforms the model to a standard system of equations for water and energy transport in unsaturated porous media [*Luikov and Mikhailov*, 1965]. The system is completed by a water retention function that provides a relationship between water saturation and water

pressure head. In this study we adopt the Brooks and Corey model [*Brooks and Corey*, 1966]:

$$\begin{aligned} &\psi_w - \psi_a = P_c(S_w),\ P_c(S_w) = \psi_s S_w^{-b}, \quad \psi_w \le \psi_s, \\ &S_w = 1, \qquad\qquad\qquad\qquad\qquad\quad \psi_w > \psi_s, \end{aligned} \tag{7}$$

where $\psi_s(<0)$ is the air entry potential and b is the Brooks and Corey model exponent. The capillary pressure function $P_c(S_w)$ is negative and increases from negative infinity to ψ_s as S_w grows to unity. In the formulation presented in this paper the air pressure ψ_a will be assumed to be zero gauge pressure. The case when soil becomes saturated ($S_w = 1$) is not of interest and will be considered only as a limiting case for the solution that is developed for unsaturated conditions.

[19] The AW zone is depicted in Figure 1 as the region to the right of the curve A–B, which is based on the thermodynamic equilibrium conditions defined by (11) in section 2.3. We note that in this region, capillary forces keep the media unfrozen even if the temperature is below 0°C but higher than the first critical temperature, $T_* < T < 0$°C. The freezing process related to the AW zone is illustrated in Figure 1 as the I–II curve.

[20] Relations (6) and (7) complete the model in the AW zone.

2.3. Unsaturated Frozen Zone (AWI Zone)

[21] In the AWI zone, ice crystals are formed but do not occupy all of the empty space within a pore void. This allows ice to grow without resistance for expansion, and therefore, we can pose a statement that the ice pressure holds zero within this zone:

$$\psi_i = 0. \tag{8}$$

[22] *Miller* [1980] suggested that drying and wetting phenomena in ice-free unsaturated soils are very similar to freezing and thawing phenomena in air-free frozen soils. In simple terms, as soil pores drain or dry by evaporation, spaces initially occupied by water are replaced by air. In the analogy the same occurs in soils during freezing. Water now is replaced by ice instead of air. The capillary forces on the water-air interfaces resist the draining of liquid water from the pores, and in the same way the capillary forces on the water-ice interfaces resist the change of phase of the liquid water to ice. This similarity, studied by *Koopmans and Miller* [1966] and *Spaans and Baker* [1996], accounts for the use of the same water retention function for both drying-wetting and freezing-thawing phenomena. Although this consideration was primarily developed for air-free saturated frozen soils by the similitude theory, it has been widely used for unsaturated freezing soils. Assuming that ice behaves similar to air, it yields a relation similar to (7):

$$\psi_w - \psi_i = \gamma P_c(S_w). \tag{9}$$

The coefficient γ represents a ratio of specific surface energies at the air-water and ice-water interfaces. The value of γ depends on the type of soil. Under saturated conditions, *Koopmans and Miller* [1966] concluded that for colloid-free soils, $\gamma = 2.2$, while $\gamma = 1$ for colloidal soils. Given the uncertainty in defining γ and keeping the model simple enough, in this paper we set $\gamma = 1$.

[23] The presence of ice and water within the pore structure leads to the occurrence of ice-water interfaces. Following the assumption of equilibrium at any instance in the soil, we present the generalized Clapeyron equation [*Miller*, 1980]:

$$\frac{\psi_w}{\rho_w} - \frac{\psi_i}{\rho_i} = \frac{L}{\rho_w g T_f} T, \tag{10}$$

where g is the acceleration due to gravity and $T_f = 273.15$ K. Substituting zero ice pressure (8) into (9) and (10) and then combining the resulting equations into one form yields $P_c(S_w) = LT/(gT_f)$, or

$$S_w = \left(\frac{LT}{g\psi_s T_f}\right)^{-1/b}. \tag{11}$$

We note that having $\psi_s < 0$ and $T < g\psi_s T_f / L < 0$ maintains positive values of the expression on the right-hand side of (11). The power function type relationship (11) between temperature and water saturation is similar to what other studies have used as the regression fit equation for available experimental data [*Spaans and Baker*, 1996].

[24] In Figure 1, the liquid saturation in the AWI zone occurs along the line II–V′, which is expressed by the equilibrium relation (11). The freezing process shown as the variation of total water saturation follows the line II–III–IV for $T_{**} < T < T_*$. Equations (8), (9), and (11) complete the model in the AWI zone.

2.4. Saturated Frozen Zone (WI Zone)

[25] In the WI zone, there is no air present in the pore voids. This results in $S_a = 0$ and modifies (1) into

$$S_w + S_i = 1. \tag{12}$$

[26] The presence of an ice-water interface within the pore voids and with the assumption of local thermodynamic equilibrium validates the use of the generalized Clapeyron equation (10) for the WI zone. As discussed, equation (9) was originally introduced for saturated soils and is therefore valid for the WI zone. The difference with the AWI zone is that the presence of air in the voids allows space for ice to expand in a pore during the freezing process, while in the WI zone, ice needs to push out water in order to expand. Ice has a specific volume higher than water; thus, for a fixed mass of water that transforms into ice, more space is needed to accommodate the expansion, hence creating internal pore stresses. This forces ice pressure to be nonzero (positive) in the WI zone. Expressing ψ_i from (9) and substituting it into (10) yields

$$\psi_w = \frac{\rho_w}{\rho_w - \rho_i} P_c(S_w) - \frac{\rho_i}{\rho_w - \rho_i} \frac{L}{gT_f} T. \tag{13}$$

[27] In Figure 1, the WI zone is depicted as the region to the left of the AWI zone. Rather than following the equilibrium curve segment shown by V′–B as given by (11), which assumes a zero ice pressure, a departure line, shown

by V′–VI′, is followed because of the nonzero ice pressure. Equations (9), (12), and (13) complete the model in the WI zone.

[28] With supplementary thermodynamic equilibrium relations developed separately for each zone, the system of equations for freezing in partially saturated porous media is now complete and needs to be supplemented with initial and boundary conditions for each specific problem.

3. Mathematical Model

[29] A schematic of the physical system studied in this paper is presented in Figure 2. We consider a one-directional freezing of a semi-infinite horizontal unsaturated soil column in $x \in [0, \infty)$. Initially, all characteristics of the medium are uniform; the soil is unfrozen, has water saturation $S_{w\infty}$, and has ice saturation $S_i = 0$, and at temperature T_∞ greater than the freezing point of pure water in the unsaturated porous media, $T_\infty^{\min} = gT_f P_c(S_{w\infty})/L$, as given by (11). These initial conditions also characterize the system at the boundary $x \to \infty$ for $t > 0$. At $x = 0$ the freezing temperature is held constant at T_0. To ensure freezing occurs at the freezing boundary, the freezing temperature must be below the negative temperature controlled by the initial capillary pressure drop in (11): $T_0 < T_\infty^{\min}$. This results in partial freezing of water near the freezing boundary $x = 0$, which expands to the right with time while freezing proceeds. The boundary $x = 0$ is considered to be impermeable for water flow.

[30] One possible distribution of total water saturation and temperature is presented in Figure 2. The sequence of WI, AWI, and AW zones represents a logical occurrence of different zones during freezing of soil columns. Zone order is characterized by the two critical temperatures T_* and T_{**} mentioned in section 2 and the corresponding transition points x_* and x_{**}. Here it is assumed $T_0 < T_{**}$.

[31] The set of equations (1)–(3) and (5) with either equations (6) and (7) for the AW zone, equations (8), (9), and (11) for the AWI zone, or equations (9), (12), and (13) for the WI zone represents a complete system of equations to describe heat and mass transport with phase change in nonheaving freezing unsaturated soils. This system is solved for seven variables, S_w, S_i, S_a, ψ_w, ψ_i, T, and q, and is supplemented by the following initial and boundary conditions:

$$t = 0, \quad x > 0, \quad S_w = S_{w\infty}, \quad S_i = 0, \quad T = T_\infty, \tag{14}$$

$$t > 0, \quad x = 0, \quad q = 0, \quad T = T_0. \tag{15}$$

Condition (14) also characterizes the system at infinity for $t > 0$.

3.1. Nondimensionalization

[32] The mathematical model developed for the studied problem consists of two partial differential equations, a set of algebraic equations, and fixed initial and boundary conditions. This situation allows a solution to be self-similar with new coordinate in a form of $xt^{-1/2}$ and flux proportional to $t^{-1/2}$, which transforms the original system into a system of ordinary differential equations. Scaling variables with their reference values, we introduce the following nondimensional functions:

$$\xi = x\sqrt{\frac{C_m}{t\lambda_m}}, \quad Q = q\frac{\phi_t}{\phi}\sqrt{\frac{tC_m}{\lambda_p}},$$

$$\theta = \frac{T}{T_\infty}, \quad p_w = \frac{\psi_w}{|\psi_s|}, \quad p_i = \frac{\psi_i}{|\psi_s|}.$$

[33] The scaling ensures that θ, p_w, and p_i have the same sign as their respective dimensional functions. For the sake

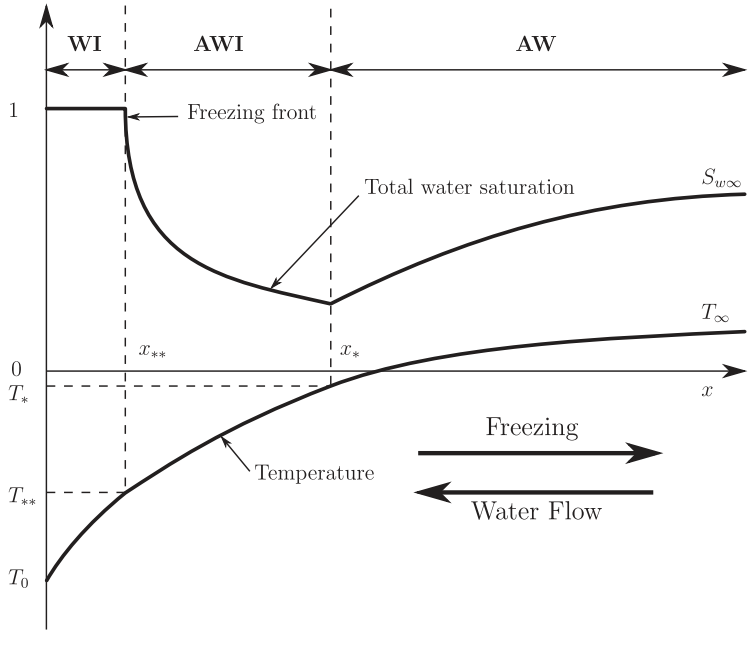

Figure 2. Schematic of total water saturation and temperature distributions during a directional freezing of a one-dimensional horizontal column. A sequence of three zones (WI, AWI, and AW) divided by the two transition points x_* and x_{**} represents a logical split of the physical domain during the freezing process.

of clarity of presentation and construction of the solution, the heat capacity C_m and the thermal conductivity λ_m are assumed to be constant, while the hydraulic conductivity K is assumed to be independent of ice with $E = 0$ for now. The influence of the parameter E will be discussed in section 5. The gravity term in (3) is also neglected as the analysis at hand is for a horizontal column. Then, the system of equations may be rewritten in nondimensional form suitable to all zones as (a prime indicates a derivative with respect to ξ)

Water balance

$$-\phi_t \frac{\xi}{2}\left(S_w' + \delta S_i'\right) + Q' = 0, \tag{16}$$

Heat balance

$$-\frac{\xi}{2}\theta' + \frac{\xi}{2} St S_i' + (Q\theta)' = \theta'', \tag{17}$$

Liquid water flux

$$Q = -\mathcal{K}(S_w) p_w', \tag{18}$$

AW zone ($\mathcal{G} < 0$)

$$p_i = 0, \quad p_w = \mathcal{P}_c(S_w), \quad S_i = 0, \tag{19}$$

AWI zone ($\mathcal{G} = 0$)

$$p_i = 0, \quad p_w = \mathcal{P}_c(S_w), \quad \theta = \varepsilon p_w, \tag{20}$$

WI zone ($\mathcal{G} > 0$)

$$\begin{aligned} &S_w + S_i = 1, \\ &p_i = p_w - \mathcal{P}_c(S_w), \\ &p_w = \mathcal{P}_c(S_w) + \frac{\delta}{1-\delta}\mathcal{G}(S_w, \theta), \end{aligned} \tag{21}$$

where

$$\mathcal{P}_c(S_w) = -S_w^{-b}, \quad \mathcal{K}(S_w) = k S_w^{2b+3},$$

$$\mathcal{G}(S_w, \theta) = \mathcal{P}_c(S_w) - \frac{\theta}{\varepsilon}.$$

The boundary conditions are expressed as

$$\xi = 0, \quad \theta = \theta_0, \quad Q = 0 \tag{22}$$

$$\xi \to \infty, \quad \theta = 1, \quad S_w = S_{w\infty}, \quad S_i = 0. \tag{23}$$

The dimensionless parameters in (16)–(21) are defined as

$$\delta = \frac{\rho_i}{\rho_w}, \quad \phi_t = \phi \frac{C_w}{C_m}, \quad St = \frac{\phi \rho_i L}{C_m T_\infty},$$

$$\varepsilon = \frac{g T_f |\psi_s|}{L T_\infty}, \quad k = \frac{K_s |\psi_s| C_w}{\lambda_m}.$$

[34] The system (16)–(21) contains six unknown functions: S_w, S_i, p_w, p_i, T, and Q. The air saturation may be found from (1). The type of zone can be determined by the function $\mathcal{G}(S_w, \theta)$, which represents any deviation from the equilibrium condition representing the AWI zone. In that regard, $\mathcal{G} < 0$ in the AW zone, the WI zone exists where $\mathcal{G} > 0$, and the AWI zone exists where $\mathcal{G} = 0$.

3.2. Weak Solution

[35] Equations (16) and (17) represent two balance equations for θ and either S_w or p_w. There is no defined transport equation for S_i since ice is assumed to be immobile. In the WI zone, $S_i = 1 - S_w$, while $S_i = 0$ in the AW zone. Substituting these expressions of S_i into balance equations (16) and (17) yields two ordinary differential equations that are of a standard parabolic type within the two-phase AW and WI zones. With known conditions at both ends of each zone, functions θ, S_w, and p_w represent continuous functions within these zones. Ice saturation is continuous in the WI zone as well. For the AWI zone θ, S_w, and p_w are related by (20), and S_i must be found as a solution of the system of equations. Substituting $p_w = \theta/\varepsilon$ from (20) into (16) and (18), eliminating θ'' by equating the resulting equation with (17), and expressing S_i' yields the following equation for the AWI zone:

$$\frac{\xi}{2}\mathcal{Q} S_i' = \frac{\xi}{2}\left[\frac{\mathcal{K}}{\varepsilon}\left(1 - \frac{S_w}{b}\right) - \frac{\phi_t S_w}{b\theta}\right]\theta' + \frac{\mathcal{K}}{\varepsilon}\left(\frac{2b+3}{b\theta} + \frac{\mathcal{K}}{\varepsilon}\right)(\theta')^2, \tag{24}$$

where

$$\mathcal{Q} = (St + \delta\phi_t\theta)\frac{k}{\varepsilon} S_w^{2b+3} + \delta\phi_t.$$

Although ice is assumed to be immobile, equation (24) may be treated as the "transport" equation for ice in the AWI zone. This differential equation is hyperbolic and may yield a weak solution, resulting in S_i being discontinuous. Since θ (also p_w and S_w through (20)) obeys the parabolic nature of equation (17), these functions are continuous in the AWI zone. To compensate for discontinuity in S_i, first derivatives of temperature, water pressure, and water saturation must also be discontinuous.

[36] According to the theory of weak solutions [*Whitham*, 1974], if the discontinuity occurs within the AWI zone at the point $\xi = \xi_d$, then two conditions can be derived at that point from the balance equations (16) and (17) as (hereafter subscript plus and minus indicate the function at the corresponding side of the discontinuity)

$$\begin{aligned} -\delta\phi_t \frac{\xi_d}{2}\left(S_i|_+ - S_i|_-\right) &= k S_{wd}^{2b+3}\left(p_w'|_+ - p_w'|_-\right) \\ (St + \delta\phi_t\theta_d)\frac{\xi_d}{2}\left(S_i|_+ - S_i|_-\right) &= \theta'|_+ - \theta'|_-, \end{aligned} \tag{25}$$

where $\theta_d = \theta(\xi_d)$ and $S_{wd} = (-\theta_d/\varepsilon)^{-1/b}$.

[37] In weak solutions the discontinuity is stable with respect to the independent variable if the stability condition written at both sides of the jump is satisfied. Applying this methodology to (24), the stability condition relates to the

function $\mathcal{Q}$. In detail, the discontinuity at any point within the AWI zone is persistent if the following conditions are met at both sides of ξ_d:

$$\mathcal{Q}|_+ > 0, \quad \mathcal{Q}|_- < 0. \tag{26}$$

If the discontinuity occurs at the end of the AWI zone where the adjacent zone is either the AW zone or the WI zone, then (26) should be satisfied at the corresponding AWI side of the jump. If (26) is not satisfied at any side of the discontinuity, then the jump in S_i is considered to be not persistent with ξ, and if it occurs, it will dissipate with ξ. For the self-similar formulation this means that a jump cannot exist at this point. The conditions (26) will be employed in construction of the solution in section 4.

4. Construction of Solution

[38] In the self-similar formulation, the soil column being unsaturated and unfrozen at the initial time dictates the existence of the AW zone for large ξ. A constant freezing temperature θ_0 forces ice to form in the soil, and either an AWI or a WI zone must exist adjacent to $\xi = 0$. The length of these two zones and the transition from one zone to another with increasing ξ cannot be assessed without having a numerical or analytical solution to the governing equations. Nonlinearity of the equation system (16)–(21) and multizone structure of solution make analytical study of the problem difficult and unattainable. Instead, having a mathematical problem formulated in a form of a system of ordinary differential equations (16) and (17) complemented with individual algebraic conditions (19)–(21) in each zone allows solving the problem as a Cauchy problem if the zone structure and the corresponding initial condition at the beginning of each zone is known. Here a trial-and-error method is used in solving the system of equations to determine the existence of the individual zones and quantify the transition between zones that do exist. The trial-and-error method consists of adjusting the initial conditions at $\xi = 0$ until the corresponding specified values of dependent variables are reached at $\xi \to \infty$. Numerical solution within each zone is based on the fifth-order Runge-Kutta method with adaptive step size control implemented in MATLAB [*The MathWorks*, 2008].

4.1. Zone Near $\xi = 0$

[39] The analysis begins with the zone adjoining the freezing boundary at $\xi = 0$. By definition that zone is either the WI zone or the AWI zone. If it is assumed that the AWI zone adjoins $\xi = 0$, then having both water pressure and water saturation being functions of temperature according to (20), a no-flow boundary condition (22) forces $\theta' = 0$ at $\xi = 0$ and makes the total number of boundary conditions to be satisfied by the heat transport equation equal to three, which is one too many. This defies the existence of a solution and, as a result, leads to the conclusion that only the WI zone can adjoin $\xi = 0$. With the existence of the WI zone next to $\xi = 0$ the conditions require only two boundary conditions to be satisfied by the heat transport equation. Another way to explain the impossibility of having the AWI zone on the boundary is that as mentioned above the no-flow boundary condition for water forces the heat flux at the boundary to be zero, and this is not physically correct as heat needs to be drawn out through the boundary to produce the freezing process.

[40] In the WI zone all variables are continuous, and $\mathcal{G} > 0$. Let ξ_{**} be the rightmost boundary of the WI zone. The coordinate ξ_{**} is found by satisfying the condition $\mathcal{G} = 0$. Within the WI zone $\xi \in [0, \xi_{**})$ functions θ and S_w are found by solving the Cauchy problem (16)–(18) and (21) with four initial conditions:

$$\xi = 0, \quad \theta = \theta_0, \quad \theta' = \theta'_0, \quad S_w = S_{w0}, \quad S'_w = \frac{\delta}{b\varepsilon} S_{w0}^{b+1} \theta'_0. \tag{27}$$

The last condition in (27) is derived from the no-flow boundary condition and (21). Values θ'_0 and S_{w0} are varied to match conditions (23) at the right boundary in the trial-and-error method.

[41] At the right end of the WI zone the temperature reaches its critical value θ_{**}. The values of θ, S_w, p_w, and p_i are found at the left side of ξ_{**} according to the equilibrium conditions (20), while ice saturation can be discontinuous:

$$\begin{aligned} &\xi = \xi_{**}|_-, \quad \theta = \theta_{**}, \quad p_i = 0, \quad p_w = \frac{\theta_{**}}{\varepsilon}, \\ &S_w = \left(-\frac{\theta_{**}}{\varepsilon}\right)^{-1/b}, \quad S_i = 1 - \left(-\frac{\theta_{**}}{\varepsilon}\right)^{-1/b}. \end{aligned} \tag{28}$$

[42] The transition to either the AWI or the AW zone must occur at ξ_{**}, and two modes of solution can be distinguished. We call it mode A if the AWI zone occurs and mode B if the AW zone occurs (see Figure 3). For either mode a discontinuity in S_i exists at ξ_{**}. As evident from (26), the discontinuity is stable if the stability condition (26) is satisfied at the right-hand side of the jump or $\mathcal{Q}(\xi_{**})|_+ > 0$. For a wide range of soil parameters, T_{**} varies from -0.5 to -3°C, which yields $\delta\phi_t|\theta_{**}|/St = C_w|T_{**}|/(\rho_w L) \ll 1$ and proves the stability condition $\mathcal{Q}(\xi_{**})|_+ > 0$.

4.2. Mode A

[43] Mode A occurs if $S_i(\xi_{**})|_+ > 0$. The AWI zone begins at ξ_{**} and extends to ξ_* ($\xi_* > \xi_{**}$). Distributions θ and S_i in this zone can be found as a solution of the Cauchy problem (16)–(18) and (20) with initial conditions for $\theta'(\xi_{**})|_+$ and $S_i(\xi_{**})|_+$ derived from (25):

$$\begin{aligned} &\xi = \xi_{**}|_+, \ \theta = \theta_{**}, \ S_i|_+ = S_i|_- + \frac{2\mathcal{K}_{**}}{(1-\delta)\xi_{**}\mathcal{Q}_{**}}\mathcal{G}'|_-, \\ &\theta'|_+ = \theta'|_- + \frac{\varepsilon}{1-\delta}\frac{\mathcal{Q}_{**} - \delta\phi_t}{\mathcal{Q}_{**}}\mathcal{G}'|_-, \end{aligned} \tag{29}$$

where $\mathcal{G}'|_- = bS_{w**}^{-b-1}S'_w|_- - \theta'|_-/\varepsilon$ and values at $\xi = \xi_{**}|_-$ are specified in (28). In this zone, water saturation is defined as $S_w = (-\theta/\varepsilon)^{-1/b}$, and water pressure is defined as $p_w = \theta/\varepsilon$.

[44] As mentioned above, at the beginning of the zone, $\mathcal{Q}(\xi_{**})|_+ > 0$. As ξ increases, temperature also increases, followed by growth of $\mathcal{Q}$ and decrease of S_i. Any discontinuity in the AWI zone is not permitted according to (26) as $\mathcal{Q}$ stays positive if applied at the left side of the jump. Therefore, S_i is continuous in the AWI zone, which ends

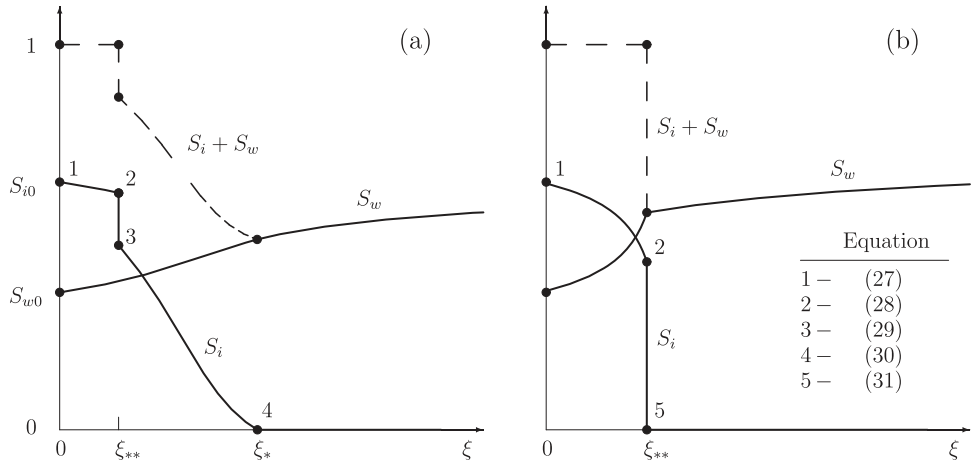

Figure 3. Profiles of ice (S_i), water (S_w), and total ($S_i + S_w$) saturations for (a) mode A and (b) mode B of the solution. Critical points in the profiles are marked with the solid circles and are labeled from 1 to 5, with the corresponding equation given in the legend. A three-zone structure occurs in mode A with two transition points, ξ_* and ξ_{**}, that envelop the AWI zone, while a two-zone structure occurs in mode B with a discontinuous transition of S_i from the WI zone to the AW zone at ξ_*.

only at a point ξ_* where S_i reaches zero. At that point the second critical temperature θ_* is reached, and the zone merges continuously into the AW zone that extends to infinity. A continuous transition of θ, S_w, and their first derivatives at ξ_* leads to a Cauchy problem for S_w and θ in the AW zone $\xi \in (\xi_*, \infty)$ with four initial conditions:

$$\xi = \xi_*|_+, \quad \theta = \theta_*, \quad \theta'|_+ = \theta'|_-, \quad S_w = \left(-\frac{\theta_*}{\varepsilon}\right)^{-1/b}, \qquad S_w'|_+ = -\frac{S_{w*}}{b\theta_*}\theta'|_-. \tag{30}$$

In the AW zone, $p_w = \mathcal{P}_c(S_w)$ and $S_i = 0$. The profiles of ice, water, and total saturations are shown schematically in Figure 3a.

4.3. Mode B

[45] In mode B, ice saturation at $\xi_{**}|_+$ is equal to zero, and the WI zone transitions straight to the AW zone. The solution can be viewed with the AWI zone degenerated into a single point $\xi = \xi_* = \xi_{**}$, where the critical temperatures θ_{**} and θ_* coincide. The solution for the WI zone in mode B is similar to the derivation of the WI zone in mode A. Also similar to mode A, the AW zone extends to infinity, and functions θ and S_w are found as solutions to the Cauchy problem (16)–(19) with initial conditions for $\theta'(\xi_{**})|_+$ and $S_w'(\xi_{**})|_+$ derived from (25):

$$\xi = \xi_{**}|_+, \quad \theta = \theta_{**}, \quad S_w = \left(-\frac{\theta_{**}}{\varepsilon}\right)^{-1/b}, \qquad \theta'|_+ = \theta'|_- - \frac{\xi}{2}(St + \delta\phi_t\theta_{**})S_i|_-, \qquad S_w'|_+ = S_w'|_- + \frac{\delta}{b}S_{w**}^{b+1}\left(\frac{\mathcal{G}'|_-}{1-\delta} + \frac{\xi_{**}}{2}\phi_t\frac{S_i|_-}{kS_{w**}^{2b+3}}\right), \tag{31}$$

where values at $\xi = \xi_{**}|_-$ are specified in (21) and (28). The behavior of the functions in the AW zone is similar to that for mode A. The profiles of ice, water, and total saturation functions are shown schematically in Figure 3b.

5. Analysis of Results

[46] The trial-and-error method of solving the Cauchy problem is based on iterative adjustment of values of S_w and θ' at $\xi = 0$ until the acceptable truncation error matching the specified values of θ_∞ and $S_{w\infty}$ at $\xi \to \infty$ is reached. The minimum value of S_w at $\xi = 0$ is specified as $S_{w0}^{\min} = (-\theta_0/\varepsilon)^{-1/b}$ by satisfying the equilibrium condition $\mathcal{G}(S_{w0}, \theta_0) = 0$, while the maximum value of S_{w0} is reached when the initial water saturation tends to unity.

[47] While solving the Cauchy problem (16)–(21), the corresponding initial conditions are employed within each zone (see Figure 3): the conditions (27) are used for the WI zone in both mode A and mode B, conditions (29) are used for the AWI zone in mode A, and for the AW zone, conditions (30) are used in mode A and conditions (31) are used in mode B. Progressing toward higher values of ξ with the Runge-Kutta method, the condition $\mathcal{G} = 0$ is used within the WI zone to identify the location of ξ_{**} and compute the first critical temperature θ_{**}. Condition $S_i = 0$ is used within the AWI zone to identify the location of ξ_* and find the second critical temperature θ_*. Two modes of solution are distinguished by the value of S_i at the right side of ξ_{**} calculated with (29). If $S_i(\xi_{**})|_+$ is positive, then mode A occurs, and initial conditions (29) are used for the Cauchy problem in the following AWI zone. Once S_i approaches zero while ξ increases in this zone, a transition to the AW zone occurs. Conditions (30) are used as initial conditions for the Cauchy problem in the AW zone. Mode B occurs if $S_i(\xi_{**})|_+$ is found by (29) to be equal or less than zero. In this case (29) is replaced with condition (31) at $\xi_*|_+$, and the AW zone extends to infinity with $S_i = 0$.

[48] Results of numerical simulations are presented for a silt loam soil [*Rawls et al.*, 1982] with the values of physical and model parameters listed in Table 1. In these simulations the initial temperature T_∞ is held equal to 1°C, while

Table 1. Dimensional and Nondimensional Model Parameters and Their Corresponding Values for Two Soils: The Silt Loam Soil Used in Construction of the Self-Similar Solution and the Silica Flour Used in the Experiment[a]

Parameter	*Rawls et al.* [1982]	*Jame and Norum* [1980]	Units
Porosity ϕ	0.49	0.49	
Air entry potential ψ_s	-0.7	-2	m
Model exponent b	5	2	m
Saturated hydraulic conductivity K_s	4×10^{-7}	6×10^{-7}	m s^{-1}
Heat capacity of soil C_m	3.2×10^{-6}	3.0×10^{-6}	J m^{-3} K^{-1}
Thermal conductivity λ_m	0.7	2	W m^{-1} K^{-1}
δ	0.918	0.918	
ϕ_t	0.64	0.683	
k	1.68	2.51	
St	46.95	8.7	
ε	5.62×10^{-3}	2.8×10^{-3}	

[a]See *Rawls et al.* [1982] for the silt loam soil, *Jame* [1977] and *Jame and Norum* [1980] for the silica flour. Values of other parameters are $\rho_w = 1000$ kg m^{-3}, $\rho_i = 917$ kg m^{-3}, $g = 9.81$ m s^{-2}, $L = 3.34 \times 10^5$ J kg^{-1}, $C_w = 4.2 \times 10^6$ J m^{-3} K^{-1}, $T_f = 273.15$ K.

values of initial water saturation $S_{w\infty}$ and freezing temperature T_0 varied. We note that results for different values of T_∞ ($> T_\infty^{\min}$) are similar to the ones presented here for $T_\infty = 1°C$.

[49] Figure 4 shows profiles of ice saturation for seven different initial water saturations and with $E = 0$. Solid curves labeled from 1 to 7 correspond to $S_{w\infty}$ equal to 0.4, 0.5, 0.6, 0.62, 0.67, 0.8, and 0.997, respectively. Mode A occurs for curves from 1 to 4, which are for smaller values of $S_{w\infty}$. With an increase of $S_{w\infty}$, mode A transitions into mode B at $S_{w\infty}^{\text{crit}} \simeq 0.67$, represented by curve 5. Mode B also occurs for curves 6 and 7. Curve 7 represents a solution for $S_{w\infty}$ being at $S_{w\infty}^{\max} \simeq 0.997$, a maximum value that is slightly less than the upper limit value of unity.

[50] With freezing temperature kept constant the initial saturation $S_{w\infty}$ needs to be large enough to satisfy the condition $\mathcal{G}(S_{w\infty}, \theta_0) > 0$ to have the freezing process occur. Otherwise, capillary forces existing initially in the system will keep water at the boundary from freezing. Solving this condition for $S_{w\infty}$ provides the minimum value of initial saturation as $S_{w\infty}^{\min} = \varepsilon^{1/b} \simeq 0.355$ for $T_\infty = -1°C$. For the values less than the minimum allowed ($0 \le S_{w\infty} < S_{w\infty}^{\min}$), the freezing does not occur, and so the whole domain consists of an AW zone. Mode A occurs for $S_{w\infty}^{\min} < S_{w\infty} < S_{w\infty}^{\text{crit}}$, while mode B occurs for $S_{w\infty}^{\text{crit}} < S_{w\infty} < S_{w\infty}^{\max}$.

[51] Two limiting cases of $S_{w\infty}$ that bound the possible range of initial water saturation, $S_{w\infty} = S_{w\infty}^{\min}$ and $S_{w\infty} = S_{w\infty}^{\max}$, and the case of initially saturated condition $S_{w\infty} = 1$ are of interest. For the case of $S_{w\infty}$ slightly departing from its minimum value $S_{w\infty}^{\min}$, a limiting case of modes A and B occurs. For that limiting case the WI zone exists

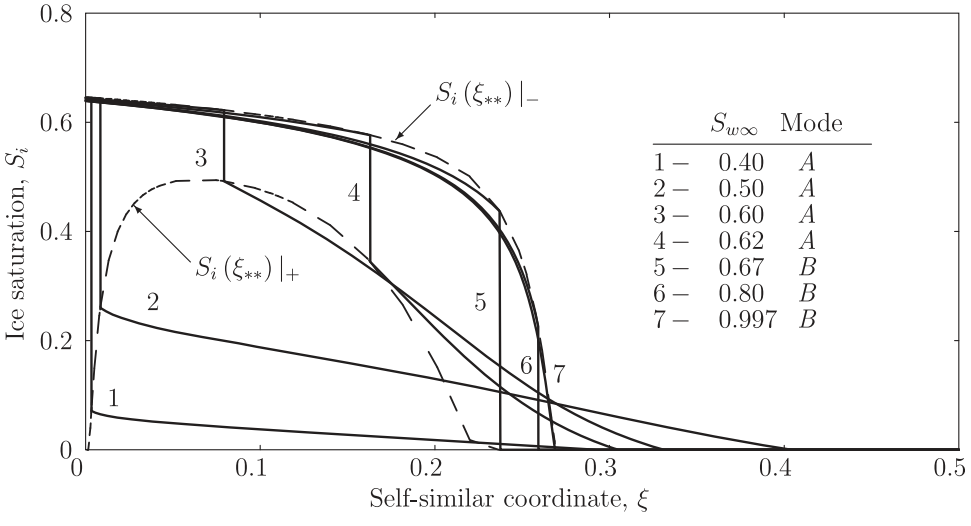

Figure 4. Distribution of ice saturation for $T_0 = -1°C$, $T_\infty = 1°C$, and different values of $S_{w\infty}$. The soil parameters used for the calculations are from *Rawls et al.* [1982], as summarized in Table 1. Curves labeled from 1 to 7 correspond to $S_{w\infty} = 0.4$, 0.5, 0.6, 0.62, 0.67, 0.8, and 0.997, respectively. The corresponding mode of the solution is also indicated. Curve 5 is for $S_{w\infty} = S_{w\infty}^{\text{crit}} = 0.67$ and represents a transitional solution from mode A to mode B. Curve 7, $S_{w\infty} = S_{w\infty}^{\max} = 0.997$, represents an upper end of the range of $S_{w\infty}$ for the validity of the governing equations. Dashed lines envelop the region of discontinuity of S_i at the transition point $\xi = \xi_{**}$.

only in one point, $\xi = 0$, such that $\xi_{**} = \xi_* = 0$. Ice, water saturation, and temperature can be expressed as

$$\begin{aligned} &\xi = 0, \quad \theta = \theta_0, \quad S_w = \left(-\frac{\theta_0}{\varepsilon}\right)^{-1/b}, \quad S_i = 1 - \left(-\frac{\theta_0}{\varepsilon}\right)^{-1/b} \\ &\xi > 0, \quad \theta = \theta_\infty, \quad S_w = \varepsilon^{1/b}, \quad S_i = 0. \end{aligned} \tag{32}$$

The value of $S_i(0)$ in (32) also represents a maximum possible value for ice saturation at the freezing boundary. An increase of $S_{w\infty}$ results in lower values of $S_i(0)$.

[52] The case of $S_{w\infty} = S_{w\infty}^{\max}$ represents an upper limit of values of $S_{w\infty}$ when water saturation reaches the saturated condition at ξ_{**}. The discontinuity at ξ_{**} vanishes in mode B, as seen in curve 7 in Figure 4, and the WI zone passes continuously into the AW zone ($\xi > \xi_{**}$), where water saturation decreases from unity at ξ_{**} to $S_{w\infty}^{\max}$ at $\xi \to \infty$. With an increase of $S_{w\infty}$ from $S_{w\infty}^{\text{crit}}$ to $S_{w\infty}^{\max}$, the water saturation profile in the AW zone transforms from a continuous increase to a decreasing function of ξ reaching a maximum at ξ_{**}. For the parameters used here, this transition occurs at $S_{w\infty} \simeq 0.96$. This transition also represents a shift in water movement in the AW zone in which flow occurs from the warm zone to the freezing front for lower values of $S_{w\infty}$ to a flow toward the warm zone from the freezing front for higher values of $S_{w\infty}$.

[53] For saturations $S_{w\infty}$ higher than $S_{w\infty}^{\max}$ the approach used in this paper to construct a solution cannot be utilized since for an initial saturation exceeding $S_{w\infty}^{\max}$ a fully saturated unfrozen zone forms between the WI and the AW zones. In this zone, water pressure exceeds the air entry value ψ_s, invalidating the basis for equation (19). An extension of the approach presented here needs to be developed to accommodate the existence of such a zone. We hypothesize that with the increase of $S_{w\infty}$ above $S_{w\infty}^{\max}$ the single point ξ_{**} where $S_w = 1$ formed at $S_{w\infty}^{\max}$ will start widening into a finite fully saturated zone, sandwiched between the WI and AW zones. The right end of this zone will expand to infinity as $S_{w\infty} \to 1$.

[54] The dynamics of the transition points ξ_* and ξ_{**} as $S_{w\infty}$ increases from $S_{w\infty}^{\min}$ to $S_{w\infty}^{\max}$ can be seen in Figure 4. Values of ice saturation at both sides of the discontinuity at ξ_{**} are shown as dashed lines. For $S_{w\infty}$ at its minimum value $S_{w\infty}^{\min}$, no freezing zone is present. An increase of $S_{w\infty}$ above $S_{w\infty}^{\min}$ results in the formation of the WI and AWI zones. These zones uniformly expand further to higher ξ while $S_{w\infty}$ increases until initial water saturation approaches a threshold value ($S_{w\infty} \simeq 0.5$). A further increase of $S_{w\infty}$ beyond this threshold leads to a shrinkage of the AWI zone while the WI zone keeps expanding. This tendency proceeds up to $S_{w\infty} = S_{w\infty}^{\text{crit}}$ at which point the AWI zone disappears and mode A of the solution transitions into mode B. Further increases of $S_{w\infty}$ lead to the growth of the WI zone until its maximum length is reached at $S_{w\infty}^{\max}$.

[55] A change in the ice accumulation at ξ_{**} with changes in $S_{w\infty}$ can be seen in Figure 4. The jump in S_i is largest for $S_{w\infty} = S_{w\infty}^{\min}$, gradually decreasing until $S_{w\infty} \simeq 0.6$, and then increasing again until the critical value $S_{w\infty} = S_{w\infty}^{\text{crit}}$ is reached. The region of S_i discontinuity is presented as an area between two dashed curves in Figure 4. The lower curve bounds the right side of the jump, while the upper curve bounds the left side of the jump.

[56] Profiles of water and total saturations, temperature, water flux, and pore stress (discussed in section 7.2) are illustrated in Figure 5 for the seven values of $S_{w\infty}$ previously introduced in Figure 4. The distribution of S_w for the case of $S_w = S_{w\infty}^{\min}$ is presented as the horizontal dotted line in Figure 5a. Profiles of S_w illustrated by solid lines in Figure 5a rise in value over the entire domain with an increase of $S_{w\infty}$ from $S_{w\infty}^{\min}$ to about 0.96. For $S_{w\infty} \simeq 0.96$ (results not plotted), S_w is constant and equal to $S_{w\infty}$ for any $\xi > \xi_{**}$, and for this value of $S_{w\infty}$ the flux to the right of ξ_{**} is zero. For initial saturations above 0.96, S_w decreases to the right in the AW zone from a maximum value at ξ_{**}. A sharp change in slope occurs at ξ_{**} because of discontinuity in S_w' and is highly pronounced in mode B in curves 5, 6, and 7. Total water saturation profiles (dashed curves) clearly show a pronounced fully saturated frozen WI zone behind the freezing zone that expands as $S_{w\infty}$ increases. Temperature profiles presented in Figure 5b exhibit steeper slopes in the freezing zones with an increase of $S_{w\infty}$. Similar to water saturation profiles, a change in temperature gradient can be seen at the transition point ξ_{**} in each curve, reflecting the release of latent heat due to the rapid change in ice content. The results for $S_{w\infty} = 0.80$ (curve 6) essentially coincide with $S_{w\infty} = 0.997$ (curve 7), so it is not plotted separately in Figure 5b.

[57] An interesting behavior of water flux is shown in Figure 5c. In cases 1 to 6, water is drawn from warmer regions (AWI and AW zones) toward ξ_{**}. With an increase of $S_{w\infty}$, the maximum flux at the left of the AW zone grows for solutions with mode A, while it decreases for solutions with mode B. Water is also drawn toward the freezing zone and to ξ_{**} from the warmer region on the right, at first increasing as $S_{w\infty}$ increases but then decreasing to zero for $S_{w\infty} \simeq 0.96$ (results not shown). For $S_{w\infty} > 0.96$, water flows toward the warm region in the AW zone from the freezing zone. For all modes, water moves toward ξ_{**} within the WI zone, and the flux increases sharply in mode B. At $S_{w\infty} = S_{w\infty}^{\max}$, shown as curve 7, water flux from the WI zone reaches its maximum value at ξ_{**} and gradually decreases to zero in the AW zone.

[58] The freezing rate in the column, the rate at which the freezing front moves, is a function of both the initial water saturation and the freezing temperature on the left boundary. Generally, the rate will increase as T_0 decreases and $S_{w\infty}$ decreases. This freezing rate is manifested in the behavior of the transition points ξ_* and ξ_{**} as a function of the initial saturation $S_{w\infty}$ and the temperature T_0. The behavior of these transition points is presented in Figure 6. The solid lines indicate the position of the tail of the freezing zone ξ_{**}, while curves for the front of the freezing zone ξ_* are shown by the dashed lines. For smaller values of $S_{w\infty}$ the majority of the domain is occupied by the AWI zone, with the WI zone being relatively small. Decreasing the freezing temperature T_0 while keeping the same initial water saturation decreases the WI zone. For values of T_0 close to 0°C the AWI zone is very small, and ξ_{**} almost coincides with ξ_*, as demonstrated by the case of $T_0 = -0.1$°C. The stronger the freezing conditions applied at the boundary are as indicated by the lower T_0, the farther the AWI zone can expand in mode A, while the WI zone advances farther in mode B for higher values of $S_{w\infty}$. With an increase of $S_{w\infty}$ for $T_0 < -2$°C, a rapid growth of the

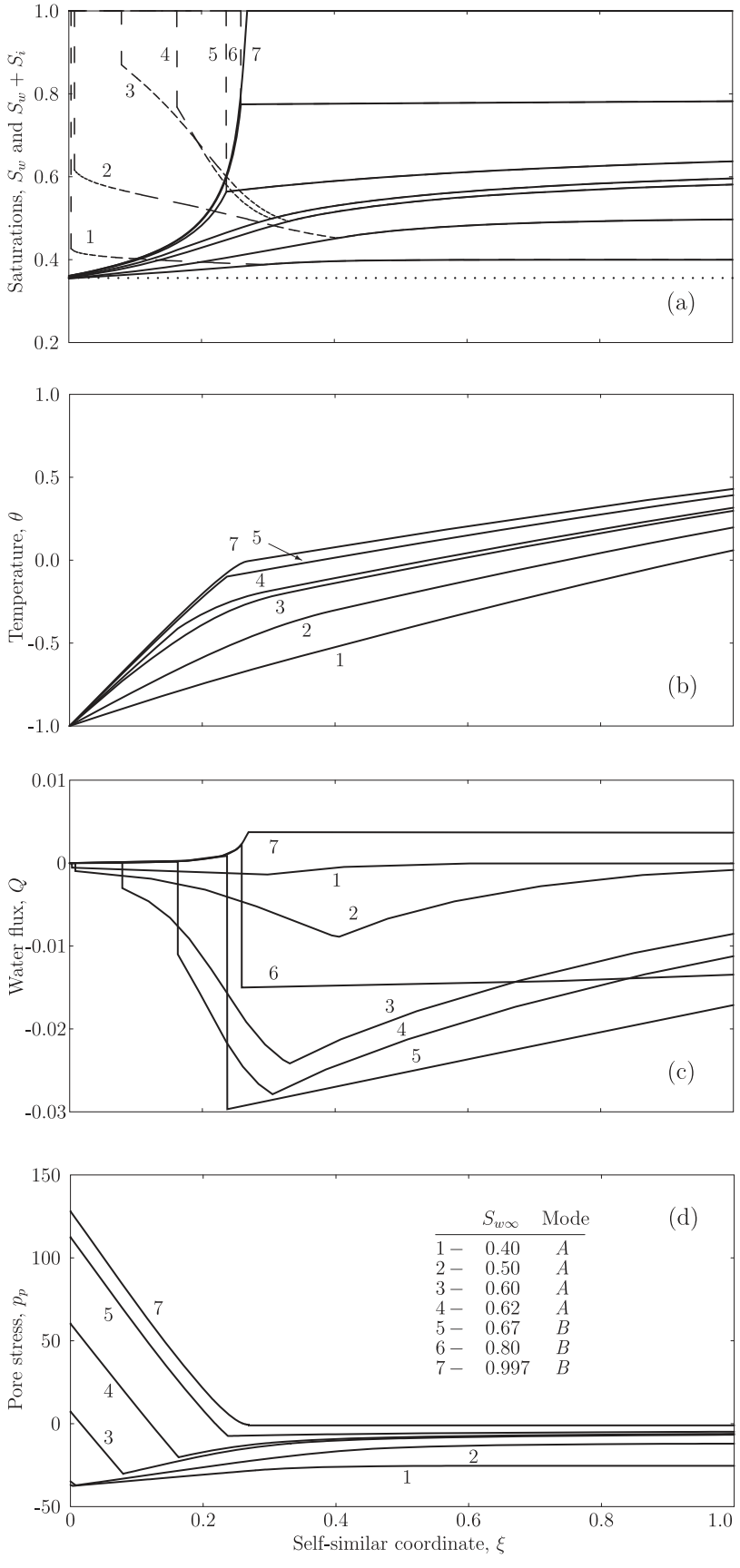
Saturations, S_w and $S_w + S_i$
Temperature, θ
Water flux, Q
Pore stress, p_p
Self-similar coordinate, ξ
(a)
(b)
(c)
(d)
$S_{w\infty}$ Mode
1 – 0.40 A
2 – 0.50 A
3 – 0.60 A
4 – 0.62 A
5 – 0.67 B
6 – 0.80 B
7 – 0.997 B

Figure 5

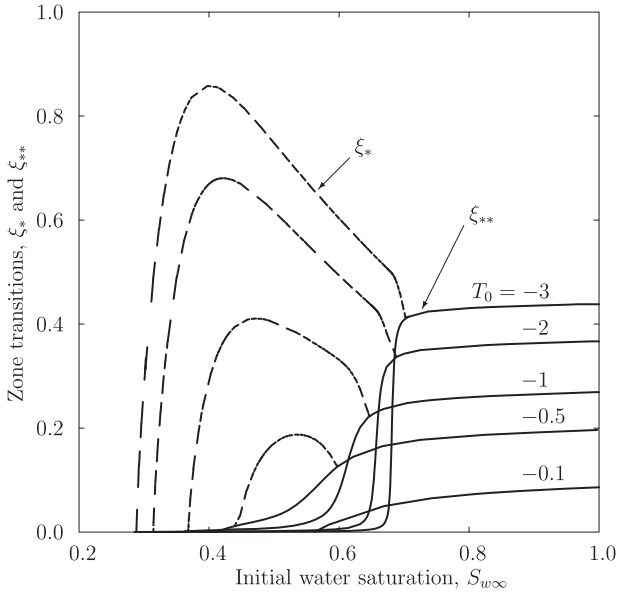

Figure 6. Transition points ξ_* (dashed lines) and ξ_{**} (solid lines) versus initial water saturation for $T_\infty = 1°C$ and various freezing temperatures T_0.

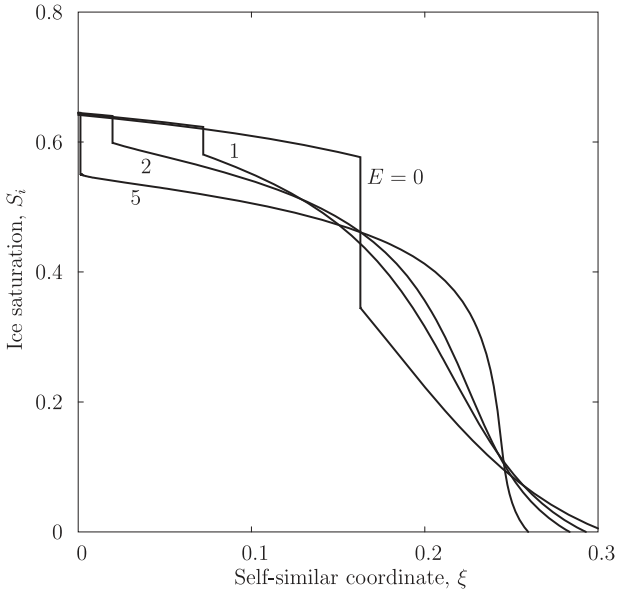

Figure 7. Impact of impedance factor E on distribution of ice saturation. The curves are plotted for $T_0 = -1°C$, $T_\infty = 1°C$, $S_{w\infty} = 0.62$, and four values of E (0, 1, 2, and 5). A solution for the values of E higher than 5 was unattainable with the framework presented in this study, as the WI zone diminishes to zero and $S_i'(\xi_{**})|_+$ tends to infinity.

frozen saturated (WI) zone is observed near the merging point of ξ_* and ξ_{**}, where the transition from mode A to mode B occurs. A small variation in $S_{w\infty}$ leads to rapid expansion of the WI zone with a collapse of the AWI zone. The rapid growth of the WI zone can also be seen in Figure 4 while moving from curve 3 to curve 5 by changing $S_{w\infty}$ from 0.6 to 0.67.

[59] Results presented up to this point were developed for the case $E = 0$. As discussed in section 2, the impedance factor E is included in (4) to lower the hydraulic conductivity due to ice blockage of continuous flow paths. This effect limits the liquid water flow and thereby significantly affects the freezing process. As an example of the impact that the impedance factor may have on the solution, Figure 7 shows ice saturation distributions for various values of E. All model parameters are taken from Table 1, and simulations are conducted for $S_{w\infty} = 0.62$ (see Figure 4 for comparison). The flux toward the tail of the freezing zone is reduced as E increases, and this results in faster ice accumulation in the AWI and reduction of the WI zone. This situation is analogous to the previously presented case with $E = 0$ while decreasing initial water content. For values of E larger than 5, the WI zone diminishes to zero, and $S_i'(\xi_{**})|_+ \to -\infty$, as seen from (24) with $\xi \to 0$. In this case, to preserve convergence of the Runge-Kutta method the step size in ξ was reduced to values smaller than the minimum computer precision, thus making completion of numerical calculations impossible. On the basis of these results it is clear that for the extreme case of $E \to \infty$, there will be no water redistribution within the freezing zones.

6. Comparison With Experiment

[60] *Jame and Norum* [1980] conducted an experiment on freezing of an initially unsaturated horizontal soil column (#40 silica flour with 72% passed through a #325 sieve) that was 30 cm in length. The retention properties of the soil used in the self-similar model are summarized in Table 1 and were adjusted to fit the relationship between the unfrozen water content and temperature presented by *Jame and Norum* [1980]. While some parameters were documented to be significantly variable with water content, such as thermal conductivity and heat capacity of soil, in our analysis they were assumed to be constant for the sake of consistency with the model formulation. The boundary conditions for the column are slightly different from those used in the self-similar solution. In the case of the experiment the boundary at the right is not at infinity, and the water flux was set to zero. Test 2 presented by Jame and Norum was held for 72 h, with temperature and total moisture profiles observed at 6, 12, 24, and 72 h after the start of the experiment. The uniform initial water content was at

Figure 5. Profiles of (a) liquid water saturation (solid lines) and total saturation (dashed lines), (b) temperature, (c) water flux, and (d) pore stress, with labels from 1 to 7 corresponding to $S_{w\infty} = 0.4$, 0.5, 0.6, 0.62, 0.67, 0.8, and 0.997, respectively. The profiles of ice saturation are presented in Figure 4 for the same values of $S_{w\infty}$. Dashed lines in Figure 5a represent the total water saturation ($S_i + S_w$) and diverge from the solid lines at ξ_{**} that represent the water saturation S_w. For curve 7, the $S_w = 1$ at ξ_{**} and decreases to 0.997 at $\xi \to \infty$, and the water flux decreases to the right of ξ_{**} and becomes zero as ξ approaches infinity. Distributions of temperature and pore stress for case 6 appear to be very close to curve 7 and are not shown.

15% of dry weight, or $S_{w\infty} \simeq 0.41$. To introduce a freezing temperature of $\sim -6°C$ gradually, the drop from the initial condition of $\sim 4°C$ was applied gradually within the first 4 h. The freezing front was formed soon after the beginning, and the induced water flow from the warm end started to lower moisture content ahead of freezing after about 6 h. The total moisture content behind the freezing front was relatively constant, apparently because of a lack of water movement in the freezing zone.

[61] To match results of the experiment with the self-similar solution constructed in section 4, the (x, t) coordinates for the observed times of 6, 12, 24, and 72 h were transformed into the self-similar coordinate ξ. Since the experimental column was of finite length, the larger the observed times, the shorter the column domain in the ξ coordinate. Measured values of total saturation $(S_i + S_w)$ at 6, 12, 24, and 72 h presented in Figure 8 show an approximate decrease of 5%, 10%, 17%, and 41% over the initial value of 0.41 at the warm end of the column, respectively. Within the level of the reported 20% accuracy for the experimental measurements, these values indicate that the measured moisture distributions exhibit close to self-similar behavior up to the 24 h observation time. Observations for times later than 24 h showed a significant decrease in water content at the warm end of the column, mainly because of the redistribution of water resident at the warm end.

[62] Total water contents behind the freezing front fluctuate over the value of 0.55 for all measurements, thus demonstrating similar freezing and water redistribution behavior in the frozen zone. The position of the freezing front for the times of 6, 12, and 24 h remains steady at $\xi_* \sim 0.56$, while for the 72 h time the freezing front is at ~ 0.42, having advanced farther in terms of the dimensional coordinate x and therefore having advanced close to the warm end of the column. Since the column has finite length, the supply of water from the warm end is limited, so after a sufficient period of freezing, the supply of liquid water in the warm end will have decreased significantly. Once that saturation drops below the critical saturation for freezing, the freezing front will halt. This condition violates the similarity assumptions of the self-similar solution, and therefore, the observations at these times cannot be used in the model comparison.

[63] The self-similar transformed experimental data between 6 and 24 h are compared with the self-similar solution presented by a solid line in Figure 8. The solution is found to be of mode A with the WI zone being very small, that is, $\xi_{**} \simeq 10^{-5}$, as seen from the ice saturation profile in Figure 8. The total saturation profile in the AWI zone varies slightly over the value of 0.51 and rapidly decreases to 0.26, approaching the transition point $\xi_* \sim 0.6$. The simulated temperature profile, while not presented here, exhibited a good comparison with the experimental observations.

[64] The substantial increase in ice and water contents near the cold end due to water freezing correlates to findings in reports on numerical simulations of one-dimensional freezing of soil columns [*Jame and Norum*, 1980; *Kung and Steenhuis*, 1986; *Hansson et al.*, 2004]. The effect seen in Figure 8 is expected to be present in well-drained, colloid-free soils. Such soils have relatively sharp water retention curves. In colloidal soils (soils with significant silt and/or clay), which have water retention curves with a more gradual $P_c(S_w)$ function, the same behavior observed in Figure 8 is likely for the case of rapid freezing, while for gradual freezing the WI zone is likely to be significant in size.

7. Discussion

7.1. Morphology of the Freezing Zone

[65] The freezing front is normally associated with the progression of a zone of freezing within which a substantial increase in ice content occurs. The freezing zone behind the ice front can be either of a finite length with a gradual increase in ice content followed by a sudden increase in ice content ($\xi_{**} < \xi_*$) or simply represented by a point with a discontinuity in ice content ($\xi_{**} = \xi_*$).

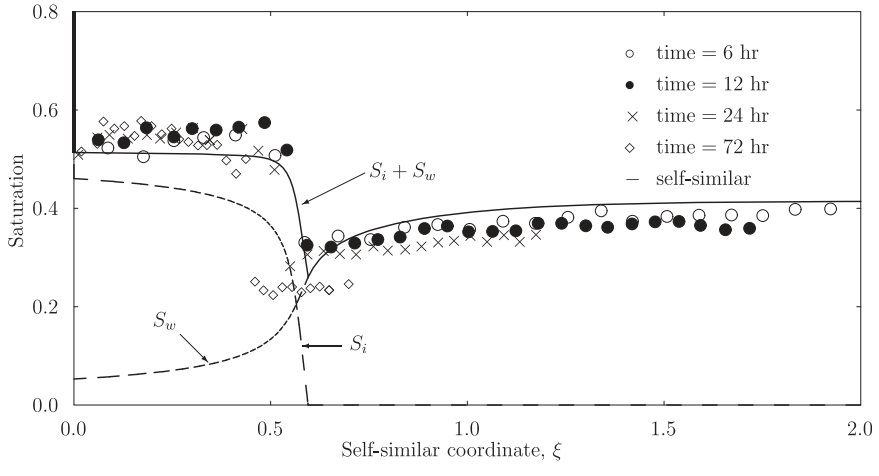

Figure 8. Total water saturation $(S_i + S_w)$ for the times of 6 h (open circles), 12 h (solid circles), 24 h (crosses), and 72 h (diamonds) observed in test 2 of *Jame and Norum* [1980] and simulated with the self-similar solution (solid line). The dashed curves present ice (S_i) and water (S_w) saturation profiles obtained with mode A of the self-similar solution. The WI zone is very small and bounded by $\xi_{**} \simeq 10^{-5}$. Values of the parameters used in the simulation are presented in Table 1.

[66] The solution constructed in section 4 showed that the fully saturated frozen WI zone must exist adjacent to the freezing boundary. The length of the zone depends on values of model parameters, initial conditions, and boundary conditions. For the case of silt loam soil presented in section 5, the zone is relatively long for mode B, while it is shorter for mode A. For mode A, a sudden increase in ice content occurs at the transition point ξ_{**}, while ice content changes continuously in between points ξ_{**} and ξ_* (the AWI zone). For mode B, the front of the freezing zone coincides with the tail (the two transition points coincide, $\xi_{**} = \xi_*$) with a substantial jump in ice content at that point. As pointed out in section 5, when initial water saturation reaches the maximum value of $S_{w\infty}^{\max}$ the jump at ξ_{**} degenerates, and a single fully saturated unfrozen point forms at ξ_{**}. For $S_{w\infty}$ higher than $S_{w\infty}^{\max}$, a finite unfrozen fully saturated zone is hypothesized to form at the warm side of the frozen zone.

[67] The size of ξ_{**} relative to ξ_* and whether the jump in ice content at ξ_{**} is substantial or not depend on the conditions set for soil parameters, boundary temperature, and initial saturation. For the results presented for the silt loam soil in Figure 4 the jump in ice content at ξ_{**} is considerable for the cases labeled as mode B, and the WI zone occupies a substantial distance. For the lower initial saturations, seen in curves 1 and 2, the jump at ξ_{**} is also pronounced, but the size of the WI zone is small compared to the AWI zone. The cases shown in Figure 4 with intermediate initial saturation lead to a much lower ice content jump at ξ_{**} and a more substantial increase in ice content in the AWI zone.

[68] Other factors are also important in controlling the relative size of the WI zone compared to the AWI zone. One important factor is the E parameter in the hydraulic conductivity function. This factor controls the redistribution of water in the freezing zone by slowing the migration of water with the increase of E. Therefore, the higher E is, the smaller the amount of water is that can be transported from the warm side of the column and through the freezing zone toward the front at ξ_{**}. This forces the freezing zone to extend farther into the warm region while making the WI zone smaller and the AWI zone larger. The effect of that parameter on the jump in ice content at ξ_{**}, the increase in ice content in the AWI zone, and the relative size of the WI and AWI zones is shown in Figure 7. It is seen from Figure 7 that as E increases, the relative size of the WI zone decreases and the relative jump in ice content at ξ_{**} decreases, only to be compensated for by increases in the length of the AWI zone and an increase in the relative ice content produced in the AWI zone.

[69] Soil texture also has a significant effect on the makeup of the frozen zones. The results in Figure 4 are for a silt loam soil, one that has a relatively gradual $P_c(S_w)$ relation. Sandy soils will have much steeper $P_c(S_w)$ relations and, as a result, a steeper $S_w(T)$ function in (11). The same drop in water content for sandy soils occurs over a much smaller difference in temperatures than for poorly drained soils, hence reducing the ability of water to migrate toward the WI zone. An example of the effect of the steeper retention relation on the morphology of the freezing zone was illustrated for the *Jame and Norum* [1980] experiment. For that case the WI zone was extremely thin.

7.2. Frost Heave

[70] Although the process of ice lens formation is not addressed in this paper, it is of interest to quantify the pore pressures that will exist within the porous medium under freezing conditions. The development of these pore pressures in the column will be discussed in section 7.2. As shown in section 2, in the AW zone no ice is present, the liquid water pressure is negative, and the air pressure is assumed to be zero. In the AWI zone the water pressure is again negative, the ice pressure is zero, and the air pressure is also zero. In the WI zone the air is absent, the ice pressure is positive, and the water pressure can be negative or positive. It is the pore pressure in the WI zone that determines whether or not the porous medium will break and frost heave will occur. Ideas about ice lens initiation and growth were discussed by *O'Neill and Miller* [1985], and the model was developed to describe frost heave and initiation of consecutive ice lenses in one-dimensional freezing of a vertical saturated soil column. Following the Terzaghi equation, total stress at any point in the soil is expressed as a sum of effective stress and pore stress, or "neutral" stress. Effective stresses represent stresses borne by the intergranular interaction of the porous matrix to support a part of the overburden pressure. The remainder of the overburden pressure is supported by pore stresses. For unsaturated freezing soils, both water and ice stresses contribute to the pore stress. *Snyder and Miller* [1985] proposed that pore stress ψ_p may be expressed by a weighting of the water ψ_w and ice ψ_i stresses as

$$\psi_p = \chi\psi_w + (1-\chi)\psi_i. \tag{33}$$

The dimensionless pore pressure is expressed as $p_p = \psi_p/|\psi_s|$. The stress partitioning coefficient χ is a function of water and ice contents and should be evaluated on the basis of experimental data. In this study we set χ as a power function of S_w: $\chi = S_w^{1.5}$ [*O'Neill and Miller*, 1985].

[71] Once the pore stresses exceed the overburden pressure at any location within the soil, the effective stresses will become zero, and the continuous pore structure of the soil breaks up, allowing the initiation of a pure ice layer at that location. This condition can be used as a limiting condition for the validity of the model presented here since as discussed in section 1, the formulation presented in this paper is valid for a rigid porous medium and therefore cannot be applied to the case of pure ice lens formation. Model limitations can be evaluated by examining the pore stresses ψ_p. It is limited to the condition where the pore stress ψ_p is less than the overburden stress.

[72] Profiles of dimensionless pore stress $p_p(\xi)$ are presented in Figure 5d for various $S_{w\infty}$. Dimensionless pore stresses are negative within the AW and AWI zones and reach positive values within the WI zone only for sufficiently moist initial conditions. From the simulation results, it is concluded that the highest positive value of the function $\psi_p(\xi)$ is at the freezing boundary $\xi = 0$. It is this value that should be compared to the overburden pressure in determining the validity of the developed model.

[73] Dimensionless pore stress at the freezing boundary $p_p(0)$ is plotted in Figure 9 as a function of $S_{w\infty}$ for various

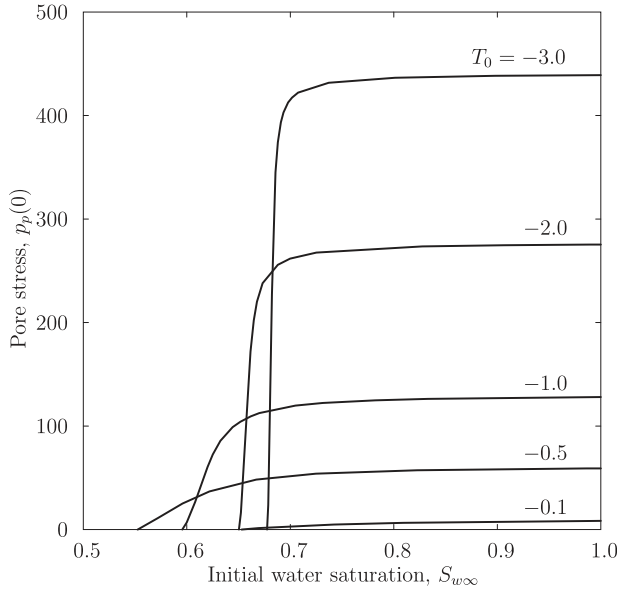

Figure 9. Profiles of pore stresses p_p at the freezing boundary $\xi = 0$ as functions of initial water saturation $S_{w\infty}$ for $T_\infty = 1$ and various values of freezing temperature. The negative side of the profiles is not shown.

freezing temperatures for the same parameters used to construct Figure 5d. For lower values of initial water saturation $S_{w\infty}$, where mode A is likely to occur, pore stresses are calculated to be negative, as exhibited by curves 1 and 2 in Figure 5d, and the model exhibits no potential for ice lens formation. Rapid growth of the WI zone within the transition from mode A to mode B with an increase of $S_{w\infty}$ correlates to rapid growth in $p_p(0)$. The pore stresses can be very high. As an example, for initially moist soils a dimensionless pore stress value of 71 can be achieved even for moderate freezing temperatures of -0.5°C. The dimensional pore stress for this case is 50 m, using the value of $\psi_s = -0.7$ m. Figure 9 indicates that lower freezing temperatures and higher initial saturation lead to more likely conditions for the occurrence of frost heave.

[74] Under actual ground-freezing conditions, ice lenses are known to form under the surface, causing soils to heave [*O'Neill*, 1983]. As shown mathematically by *O'Neill and Miller* [1985] and further expanded by *Fowler* [1989] and *Fowler and Krantz* [1994], in a vertical dimension, pore stresses reach maximum values at a point below the surface but not at the freezing surface as appeared for the case studied in this paper. At that maximum point the ice lens forms and a primary frost heave begins. As freezing progresses, the warmest side of the ice lens becomes the new upper boundary for the one-dimensional freezing problem, and the process of the pore stress buildup is repeated at a new depth, causing formation of a new ice lens. The phenomenon of such recurrent formations of ice lenses is known as the secondary frost heave [*O'Neill*, 1983].

[75] The formulation studied in this paper is different from the problem of soil frost heave described by *O'Neill and Miller* [1985]. In their formulation, O'Neill and Miller held the ice pressure at the freezing boundary constant and equal to the overburden pressure. This, in essence, then allows ice to leave the domain through the freezing boundary, thereby relieving the system from building ice pressure right at the freezing boundary. In contrast to their formulation, the formulation given in this paper satisfies the conditions imposed in the laboratory experiment of *Jame and Norum* [1980]. In that case, the system is considered closed, and a no-flow boundary condition is enforced at the freezing boundary. This boundary condition then facilitates the formulation of a self-similar solution, leading to the result that the maximum pore pressure occurs at the freezing boundary rather than inside the domain as found by *O'Neill and Miller* [1985].

[76] While the present formulation presented in this paper does have the limitation that it assumes the soil to be rigid, this is not an insurmountable obstacle to future progress. Expanding the formulation by coupling in the equations for porous media deformation will remove the assumption of porous media incompressibility. Such a system of equations is not amenable to the self-similarity formulation, but rather needs to be solved numerically.

8. Summary and Conclusions

[77] In this paper, we have presented a formulation of a mathematical model for freezing of unsaturated soils under nonheaving conditions. The model consists of heat and water mass balance equations with sets of constitutive relationships within three zones, AW, AWI, and WI, that correspond to the proportions of ice, water, and air within pore voids. The AW zone is unsaturated and unfrozen, the AWI zone is unsaturated and frozen, and the WI zone is saturated and frozen. We analyzed qualitative properties of the solution in the self-similar formulation and developed a method for solving the system of ordinary differential equations using a Runge-Kutta method. Depending on the properties of the soil and values of model input parameters, the solution leads to two modes, mode A and mode B, both of which are defined by the distribution of ice, water, and air. The mode that occurs in a given situation depends largely on the freezing rate. Whether this rate is considered to be high, medium, or low depends on the moisture retention and flow transmission properties of the particular porous medium, on the initial moisture saturation, and on the temperature at the freezing boundary. The distribution associated with mode A is composed of the WI zone near the freezing boundary, followed by the AWI zone, with the AW zone next to the AWI zone. The mode A distribution occurs for conditions associated with a relatively high freezing rate. The mode B distribution has the WI zone near the freezing boundary, followed by the AW zone, and it occurs for the conditions of a relatively low freezing rate.

[78] The leading edge of the freezing zone is formed by either the abrupt change in ice content at the boundary between the WI zone and the AW zone in mode B, or it corresponds to the boundary between the AWI zone and the AW zone for the mode A condition. The length of the WI zone and the change in ice content at the warm side of this zone are both relatively large for the mode B condition. For the mode A condition the length of the WI zone is relatively small, while the change in ice content at the warm boundary of the zone can be large or small. When this change in ice content is large, the change in ice content within the adjoining AWI zone is small and vice versa.

[79] Pore pressure within the porous medium is defined by a linear combination of the water pressure and the ice pressure. The pore pressure is negative in the AWI zone because the ice pressure is set to zero in that zone. In the WI zone the ice pressures can become positive. When the WI zone is relatively thin, the ice pressures will be small, so the pore pressures will remain negative. However, as the WI zone increases in length, the ice pressures can become large, possibly leading to positive pore pressures in excess of the overburden pressure, a condition necessary to initiate the formation of ice lenses. Ice lens formation was not considered in this paper because the porous medium was assumed to be rigid; however, the pore pressure calculation provides the limit to the validity of the self-similar solution presented.

[80] The self-similar solution was derived for a freezing experiment conducted by *Jame and Norum* [1980]. It was determined that the distribution of ice and liquid water in the experimental column was consistent with a mode A type of distribution with a very thin WI zone. The results of the self-similar solution compared favorably to the experimental observations.

[81] The derived self-similar solution can be used as a test for the validation of numerical schemes developed as simulation modules for seasonal freezing and thawing in soils in available hydrological models. An upper limit on the initial saturation exists for the solution presented. This limit is system parameter (boundary freezing temperature and soil properties) dependent. For initial saturation exceeding this upper limit the self-similar solution does not apply. For such cases a numerical solution of the governing equations will be necessary to provide valid results. Possible future extensions of this present work should be to include porous media deformation to facilitate the simulation of ice lens formation and frost heave processes.

[82] **Acknowledgments.** The authors are grateful to Andrey G. Egorov of Kazan State University, Russia, for discussions and valuable comments regarding the methods used in the study. Comments on the manuscript provided by Ronnie Daanen and two other anonymous reviewers are greatly appreciated.

References

Beskow, G. (1935), *Soil Freezing and Frost Heaving With Special Application to Roads and Railroads*, *Sver. Geol. Unders., Ser. C, 375*. [Reprinted in *Historical Perspectives in Frost Heave Research: The Early Works of S. Taber and G. Beskow*, edited by P. B. Black and M. J. Hardenberg, translated from Swedish by J. O. Osterberg, *Spec. Rep., 91-23*, pp. 37–157, U.S. Army Cold Reg. Res. and Eng. Lab., Hanover, N. H., 1991.]

Bronfenbrener, L., and E. Korin (1999), Two-phase zone formation conditions under freezing of porous media, *J. Cryst. Growth*, *198-199*, 89–95.

Brooks, R. H., and A. T. Corey (1966), Properties of porous media affecting fluid flow, *J. Irrig. Drain. Div. Am. Soc. Civ. Eng.*, *92*, 61–88.

Cary, J., and H. Mayland (1972), Salt and water movement in unsaturated frozen soils, *Soil Sci. Soc. Am. Proc.*, *36*, 549–555.

Cherkauer, K., and D. Lettenmaier (1999), Hydrologic effects of frozen soils in the Upper Mississippi River basin, *J. Geophys. Res.*, *104*(D16), 19,599–19,610, doi:10.1029/1999JD900337.

Daanen, R. P., D. Misra, and H. Epstein (2007), Active-layer hydrology in nonsorted circle ecosystems of the arctic tundra, *Vadose Zone J.*, *6*(4), 694–704.

Dirksen, C., and R. D. Miller (1966), Closed-system freezing of unsaturated soil, *Soil Sci. Soc. Am. Proc.*, *30*, 168–173.

Engelmark, H., and U. Svensson (1993), Numerical modelling of phase change in freezing and thawing unsaturated soil, *Nord. Hydrol.*, *24*, 95–110.

Flerchinger, G. N., and K. E. Saxton (1989), Simultaneous heat and water model of a freezing snow-residue-soil system 1. Theory and development, *Trans. ASAE*, *32*(2), 565–571.

Fowler, A. C. (1989), Secondary frost heave in freezing soils, *SIAM J. Appl. Math.*, *49*(4), 991–1008.

Fowler, A. C., and W. B. Krantz (1994), A generalized secondary frost heave model, *SIAM J. Appl. Math.*, *54*(6), 1650–1675.

Guymon, G. L., and J. N. Luthin (1974), A coupled heat and moisture transport model for arctic soils, *Water Resour. Res.*, *10*(5), 995–1001, doi:10.1029/WR010i005p00995.

Hansson, K., J. Simunek, M. Mizoguchi, L. C. Lundin, and M. T. V. Genuchten (2004), Water flow and heat transport in frozen soil: Numerical solution and freeze-thaw applications, *Vadose Zone J.*, *3*(2), 693–704.

Harlan, R. L. (1973), Analysis of coupled heat-fluid transport in partially frozen soil, *Water Resour. Res.*, *9*(5), 1314–1323, doi:10.1029/WR009i005p01314.

Jame, Y. W. (1977), Heat and mass transfer in freezing unsaturated soil, Ph.D. thesis, Agric. Eng. Dep., Univ. of Sask., Saskatoon, Canada.

Jame, Y. W., and D. I. Norum (1980), Heat and mass transfer in a freezing unsaturated porous medium, *Water Resour. Res.*, *18*(4), 811–819, doi:10.1029/WR016i004p00811.

Koopmans, R. W. R., and R. D. Miller (1966), Soil freezing and soil water characteristic curves, *Soil Sci. Soc. Am. Proc.*, *30*, 680–685.

Kung, S. K. J., and T. S. Steenhuis (1986), Heat and moisture transfer in a partly frozen nonheaving soil, *Soil Sci. Soc. Am. J.*, *50*, 1114–1122.

Li, Q., S. Sun, and Q. Dai (2009), The numerical scheme development of a simplified frozen soil model, *Adv. Atmos. Sci.*, *26*(5), 940–950.

Lombardi, A. L., and D. T. Tarzia (2001), Similarity solutions for thawing processes with a heat flux condition at the fixed boundary, *Meccanica*, *36*(3), 251–264.

Luikov, A. V., and Y. A. Mikhailov (1965), *Theory of Energy and Mass Transfer*, Pergamon, Oxford, U. K.

Matzner, E., and W. Borken (2008), Do freeze-thaw events enhance C and N losses from soils of different ecosystems? A review, *Eur. J. Soil Sci.*, *59*(2), 274–284.

Miller, R. D. (1973), Soil freezing in relation to pore water pressure and temperature, in *Proceedings of the 2nd International Conference on Permafrost*, pp. 344–352, Natl. Acad. Sci., Yakutsk, Russia.

Miller, R. D. (1980), Freezing phenomena in soils, in *Application of Soil Physics*, edited by D. Hillel, chap. 11, pp. 254–299, Academic, New York.

Nakano, Y., A. Tice, J. Oliphant, and T. Jenkins (1983), Transport of water in frozen soil, 2. Effects of ice on the transport of water under isothermal conditions, *Adv. Water Resour.*, *6*, 15–26.

Newman, G. P., and G. W. Wilson (1997), Heat and mass transfer in unsaturated soils during freezing, *Can. Geotech. J.*, *34*, 63–70.

O'Neill, K. (1983), The physics of mathematical frost heave models: A review, *Cold Reg. Sci. Technol.*, *6*, 275–291.

O'Neill, K., and R. D. Miller (1985), Exploration of a rigid-ice model of frost heave, *Water Resour. Res.*, *21*(3), 281–296, doi:10.1029/WR021i003p00281.

Rawls, W. J., D. L. Brakensiek, and K. E. Saxton (1982), Estimation of soil water properties, *Trans. ASAE*, *25*, 1316–1330.

Shoop, S. A., and S. R. Bigl (1997), Moisture migration during freeze and thaw of unsaturated soils: Modeling and large scale experiments, *Cold Reg. Sci. Technol.*, *25*, 33–45.

Snyder, V. A., and R. D. Miller (1985), Tensile strength of unsaturated soils, *Soil Sci. Soc. Am. J.*, *49*(1), 58–65.

Spaans, E. J. A., and J. M. Baker (1996), The soil freezing characteristic: Its measurement and similarity to the soil moisture characteristic, *Soil Sci. Soc. Am. J.*, *60*, 13–19.

Taber, S. (1930), Mechanics of frost heaving, *J. Geol.*, *38*, 303–317.

Taylor, G. S., and J. N. Luthin (1978), A model for coupled heat and moisture transfer during soil freezing, *Can. Geotech. J.*, *15*, 548–555.

The MathWorks (2008), MATLAB version 2007a, Natick, Mass.

Whitham, G. B. (1974), *Linear and Nonlinear Waves*, John Wiley, New York.

Zhao, L., D. M. Gray, and D. H. Male (1997), Numerical analysis of simultaneous heat and water transfer during infiltration into frozen ground, *J. Hydrol.*, *200*(1–4), 345–363.

J. L. Nieber, Department of Bioproducts and Biosystems Engineering, University of Minnesota, 1390 Eckles Ave., Saint Paul, MN 55108, USA. (nieber@umn.edu)

A. Y. Sheshukov, Department of Biological and Agricultural Engineering, Kansas State University, 129 Seaton Hall, Manhattan, KS 66503, USA. (ashesh@ksu.edu)